British Journal of Pharmacology

British Journal of Pharmacology (2017) **174** 628–640 628

RESEARCH PAPER

Anti-CD22 and anti-CD79b antibody-drug conjugates preferentially target proliferating B cells

Correspondence Saileta Prabhu, Department of Pharmacokinetic and Pharmacodynamic Sciences, Genentech, Inc., South San Francisco, CA, USA. E-mail: prabhu.saileta@gene.com

Received 22 June 2016; **Revised** 11 November 2016; **Accepted** 15 December 2016

Franklin K Fuh[1,*], Caroline Looney[1,*], Dongwei Li[2], Kirsten A Poon[3,8], Randall C Dere[5], Dimitry M Danilenko[4], Jacqueline McBride[1], Chae Reed[5], Shan Chung[5], Bing Zheng[6], William Rodney Mathews[1], Andrew Polson[6], Saileta Prabhu[2] and Marna Williams[1,7]

[1]Department of Pharmacodynamic Biomarkers, Genentech, Inc., South San Francisco, CA, USA, [2]Department of Pharmacokinetic and Pharmacodynamic Sciences, Genentech, Inc., South San Francisco, CA, USA, [3]Department of Safety and Toxicology, Genentech, Inc., South San Francisco, CA, USA, [4]Department of Safety Assessment, Genentech, Inc., South San Francisco, CA, USA, [5]Department of BioAnalytical Research and Development, Genentech, Inc., South San Francisco, CA, USA, [6]Department of Immunology Research, Genentech, Inc., South San Francisco, CA, USA, [7]MedImmune, Gaithersburg, MD, USA, and [8]Denali Therapeutics, Inc., South San Francisco, CA, USA

*Franklin K Fuh and Caroline Looney contributed equally to this manuscript.

BACKGROUND AND PURPOSE

CD22 and CD79b are cell-surface receptors expressed on B-cell-derived malignancies such as non-Hodgkin's lymphoma (NHL). An anti-mitotic agent, monomethyl auristatin E, was conjugated to anti-CD22 and anti-CD79b antibodies to develop target-specific therapies for NHL. The mechanism of action (MOA) and pharmacological and pharmacokinetic (PK) profiles of these antibody-drug conjugates (ADCs) were investigated in cynomolgus monkeys.

EXPERIMENTAL APPROACH

Animals were administered anti-CD22 or anti-CD79b ADCs, respective unconjugated antibodies or vehicle. Pharmacodynamic effects on total and proliferating B cells and serum PK were then assessed. Antibody-dependent cellular cytotoxicity (ADCC) and complement-dependent cytotoxicity (CDC) of the ADCs were evaluated *in vitro*.

KEY RESULTS

Depletion of B cells was observed after administration of either ADC or the respective unconjugated antibodies. An extended duration of depletion was observed in animals administered ADCs. Similarly, preferential depletion of proliferating B cells in blood and germinal centre B cells in spleen were only observed in animals administered ADCs. Serum PK profiles of ADCs and respective unconjugated antibodies were comparable. *In vitro*, anti-human CD22 and anti-human CD79b antibodies showed no or only moderate ADCC activity, respectively; neither antibody had CDC activity.

CONCLUSIONS AND IMPLICATIONS

The findings support the proposed MOA: initial depletion of total B cells by antibody-mediated opsonization, followed by preferential, sustained depletion of proliferating B cells by the auristatin conjugate due to its anti-mitotic action. Delivering potent anti-mitotic agents to B cells via the specificity of monoclonal antibodies provides a means to eliminate pathogenic B cells in NHL with improved risk–benefit profiles over traditional chemotherapeutics.

DOI:10.1111/bph.13697

Abbreviations

ADC, antibody-drug conjugate; ADCC, antibody-dependent cellular cytotoxicity; AICC, antibody-independent cellular cytotoxicity; anti-CD22, anti-human CD22; anti-huCD79b, anti-human CD79b; AUCinf, AUC extrapolated to infinity; BJAB, Burkitt's lymphoma cell line; CDC, complement-dependent cytotoxicity; Cmax, maximum serum concentration; FSC, forward scatter; GC, germinal centre; H&E, haematoxylin and eosin; mAb, monoclonal antibody; MC-VC-PAB, maleimidocaproyl-valine-citrulline-p-aminobenzyloxycarbonyl; MMAE, monomethyl auristatin E; MOA, mechanism of action; NHL, non-Hodgkin's lymphoma; NHP, non-human primate; PBMC, peripheral blood mononuclear cell; PK, pharmacokinetic/s; RT, room temperature; SSC, side scatter; TMB, tetramethylbenzidine; Vss, volume of distribution at steady state

Tables of Links

TARGETS
CD22
CD79b

LIGANDS
Rituximab

These Tables list key protein targets and ligands in this article which are hyperlinked to corresponding entries in http://www.guidetopharmacology.org, the common portal for data from the IUPHAR/BPS Guide to PHARMACOLOGY (Southan *et al.*, 2016), and are permanently archived in the Concise Guide to PHARMACOLOGY 2015/16 (Alexander *et al.*, 2015).

Introduction

B-cell lymphoproliferative disorders are heterogeneous malignancies ranging from slow-growing indolent to aggressive lymphomas. Non-Hodgkin's lymphomas (NHLs), characterized by pathogenic outgrowth of B cells, are a diverse set of malignancies that vary widely in aggressiveness and clinical outcome. NHLs are one of the most common B-cell malignancies in the United States with an incidence of over 65 000 new cases a year and continue to rise (Burton and Goldenberg, 2010).

Despite novel chemotherapeutic and monoclonal antibody (mAb) therapies (e.g. rituximab), indolent B-cell lymphomas have limited treatment options. This underscores the need for treatments that will significantly extend disease-free and overall survival in these patients. Therapies that combine the cell-targeting specificity of a mAb with the cytotoxicity of a chemotherapeutic could offer improved safety and efficacy over current therapies. Antibody-drug conjugates (ADCs) are such a new therapeutic; they are composed of a mAb conjugated to a cytotoxic agent. Treatments with ADCs that target the CD22 and CD19 antigens have shown promising results in early clinical trials in NHL (Sievers and Senter, 2013).

CD22 and CD79b are cell surface receptors whose expression is restricted to Pre-B cells and mature B cells (excluding plasma cells). CD22 and CD79b are promising targets for ADCs as they are expressed on a majority of B-cell-derived malignancies, including nearly all major subtypes of NHL (Dornan *et al.*, 2009; Polson *et al.*, 2010). CD22 and CD79b are expressed in both primary and relapsed follicular lymphoma and in diffuse large B-cell lymphoma (Dornan *et al.*, 2009; Polson *et al.*, 2010). Antibodies bound to CD22 and CD79b are rapidly internalized, which makes them ideal for targeted delivery of cytotoxic agents (Shan and Press, 1995).

We have generated anti-human CD22 (anti-CD22) and anti-human CD79b (anti-huCD79b) ADCs consisting of a mAb conjugated to a potent anti-mitotic agent monomethyl auristatin E (MMAE) via a protease-labile linker, maleimidocaproyl-valine-citrulline-p-aminobenzyloxycarbonyl (MC-vc-PAB). The linker-drug (vc-MMAE) is conjugated to the antibody through a thioether bond between the linker maleimide moiety and a cysteine thiol that forms the interchain disulfide bond in the antibody. Upon internalization, lysosomal enzymes cathepsin B and possibly other lysosomal cysteine proteases cleave the linker and release MMAE (Doronina *et al.*, 2003; Sutherland *et al.*, 2006). Once released, MMAE binds to tubulin and disrupts the microtubule network, resulting in the inhibition of cell division and growth (Polson *et al.*, 2007; Dornan *et al.*, 2009; Polson *et al.*, 2009; Zheng et al., 2009). This therapeutic approach combines the specific targeting capability and the favourable pharmacokinetics (PK) of the mAb with the cytotoxic activity of MMAE. Anti-CD22 and anti-huCD79b ADCs kill NHL cell lines *in vitro* and are effective in mouse xenograft models of NHL (Dornan *et al.*, 2009; Polson *et al.*, 2010).

Pharmacological effects, PK profiles and the mechanism of action (MOA) of anti-CD22 and anti-CD79b ADCs were evaluated in non-human primates (NHPs). As anti-huCD79b antibody does not bind to cynomolgus monkey CD79b, a surrogate anti-CD79b antibody was utilized in NHP studies. The surrogate anti-CD79b antibody/ADC resembles anti-huCD79b mAb/ADC with regard to pharmacological activity so the preclinical studies conducted with the surrogate molecule provided relevant and useful pharmacology information (Zheng *et al.*, 2009). PK profiles of anti-CD22 or anti-CD79b

ADCs were assessed in serum, and pharmacological effects on total and proliferating B cells were examined in peripheral blood and tissue. Our findings demonstrate targeted depletion of proliferating B cells by anti-CD22 and anti-CD79b ADCs, supporting the development of these ADCs to specifically target pathogenic B cells in NHL.

Methods

Test materials

Anti-CD22 ADC consists of a humanized anti-CD22 IgG1 mAb and MMAE conjugated via a protease-labile linker, maleimidocaproyl-valine-citrulline-p-aminobenzyloxycarbonyl (MC-VC-PAB). The linker-drug (vc-MMAE) is conjugated to the antibody through a thioether bond between the linker maleimide moiety and a cysteine thiol that forms the interchain disulfide bond in the antibody. The average number of MMAE molecules per anti-CD22 ADC is 3.9 (3.9 mol MMAE mol^{-1} of unconjugated anti-CD22 antibody). Anti-CD22 ADC binds to human and cynomolgus monkey CD22 with similar affinity.

Similar to anti-huCD79b ADC consists of a humanized anti-huCD79b IgG1 mAb conjugated to MMAE via MC-VC-PAB linker. The average number of MMAE molecules per anti-huCD79b ADC is 3.7 (3.7 mol MMAE mol^{-1} of the unconjugated anti-huCD79b antibody).

Anti-huCD79b ADC binds to human but not cynomolgus monkey CD79b. Therefore, a surrogate ADC, anti-CD79b that specifically binds to cynomolgus monkey CD79b, was generated. An epitope on cynomolgus monkey CD79b, to which the anti-CD79b ADC binds, is similar to that on human CD79b recognized by anti-huCD79b ADC; both ADCs have similar affinity (Zheng *et al.*, 2009). Anti-CD79b ADC consists of a chimeric anti-CD79b mouse–human IgG1 mAb conjugated to MMAE via MC-VC-PAB linker. The average number of MMAE molecules per anti-CD79b ADC is 3.5 (3.5 mol MMAE mol^{-1} of the unconjugated anti-CD79b antibody).

The respective antibody formulation buffers for anti-CD22 ADC and anti-CD79b ADC were used as vehicle (control) in all NHP studies.

Animal welfare and ethical statement

Cynomolgus monkeys (*Macaca fascicularis*) were used in these studies. Animals were treated in compliance with regulations outlined in the USDA Animal Welfare Act and the conditions specified in The Guide for Care and Use of Laboratory Animals (Institute of Laboratory Animal Research, 1996). Animal studies are reported in compliance with the ARRIVE guidelines (Kilkenny *et al.*, 2010; McGrath and Lilley, 2015). All animals were purpose bred and experimentally naïve at the outset of the studies. Prior to study assignment, animals were quarantined, maintained and monitored for good health in accordance with testing facility SOP and/or as mandated by the Centers for Disease Control and Prevention, Atlanta, Georgia. Environmental controls in the animal rooms were set to maintain a temperature of 18–29°C (64–84°F), a relative humidity of 30–70%, minimum fresh air changes of 10 h^{-1} and a light/dark cycle of 12:12 h. All animals were housed individually in stainless-steel cages but were allowed to comingle to provide psychological enrichment. Prior to dosing, animals were allowed to acclimatize to their housing for a minimum of 1–2 weeks. Foods, certified primate diets, were provided daily along with fruits or vegetable supplements 2–3 times a week. Water was provided *ad libitum* to each animal via automatic watering devices. Studies were conducted following the standard operating procedures applicable to the Clinical Research Organization (Covance, Inc. or Charles River Laboratories International, Inc.). No animals were scheduled to be killed at the end of the anti-CD22 ADC and anti-CD79b ADC studies. For histopathology, animals from separate independent studies were killed under deep (and unrecoverable) anaesthesia induced with ketamine and Nembutal or the equivalent, followed by exsanguination. All surviving animals were returned to the testing facility animal stock colony at the end of the studies.

Single-dose pharmacokinetic/pharmacodynamic studies

Anti-CD22 ADC study. Twelve male cynomolgus monkeys of Mauritian origin were obtained by Covance Laboratories Inc. (Madison, WI, USA). Animals were 3–5 years old and weighed 2.5–4 kg. All animals were verified for binding to the anti-CD22 antibody before the start of the study. Animals were assigned to three groups (four animals per group) by a stratified randomization scheme designed to achieve similar group mean body weights. The groups were then randomly assigned to administration of vehicle (control), 3 mg kg^{-1} unconjugated anti-CD22 antibody or 3 mg·kg^{-1} anti-CD22 ADC. Test and control substances were administered by a single i.v. bolus injection on Day 1. Peripheral blood samples for flow cytometry were collected pre-dose on Days −14 and −7 and post-dose on Days 2, 8, 15, 22, 29 and 44. Blood samples for PK analysis were collected at pre-dose on Day −1 and post-dose at 0.083, 4 and 12 h and on Days 2, 4, 8, 15, 22, 29, 36 and 44.

Anti-CD79b ADC study. Twelve male cynomolgus monkeys of Chinese origin were obtained by Charles River Laboratories International, Inc (Reno, NV, USA). Animals were 2–4 years old and weighed 2–4 kg. Animals were assigned to three groups (four animals per group) by a stratified randomization scheme designed to achieve similar group mean body weights. The groups were then randomly assigned to administration of vehicle (control), 3 mg·kg^{-1} unconjugated anti-CD79b antibody, or 3 mg·kg^{-1} anti-CD79b ADC. Test and control substances were administered by a single i.v. bolus injection on Day 1. Peripheral blood samples for flow cytometry were collected pre-dose on Days −8 and −1 and post-dose on Days 2, 8, 15, 22, 29 and 43. Blood samples for PK analysis were collected pre-dose on Day −8 and post-dose at 0.083, 4 and 12 h and on Days 2, 4, 8, 15, 22, 29, 36 and 43.

Assessment of anti-CD22 and anti-CD79b antibody binding to cynomolgus monkey B cells

Binding of anti-CD22 antibody to cynomolgus monkey $CD20^+$ B cells was evaluated by flow cytometry using fluorescently labelled anti-CD22 antibody. As a positive control, samples were co-stained with fluorescently labelled Hu8G10

antibody (Genentech, Inc.). This antibody binds to human and cynomolgus monkey CD22 in the presence of the anti-CD22 clinical candidate antibody (data not shown).

To assess binding of anti-CD22 antibody to cynomolgus monkey B cells, peripheral blood from animals of Chinese, Cambodian, Mauritian and Indonesian origins was collected and treated with BD PharmLyse (BD Biosciences, San Jose, CA, USA) following the manufacturer's protocol. The samples were then washed in ice-cold FACS staining buffer (composed of PBS with 2% FBS) and blocked with heat-inactivated human serum. Saturating concentrations of fluorescently labelled antibodies (anti-CD20 PE and anti-CD22 Alexa 647) and/or corresponding isotype controls (BD Biosciences) or Hu8G10 FITC (Genentech, Inc.) were then added to samples followed by incubation on ice for 25–35 min. Before acquisition, samples were washed twice with FACS staining buffer and resuspended in fixative buffer (PBS with 1% paraformaldehyde). Ten thousand lymphocyte-gated events were acquired using a forward scatter (FSC)/side scatter (SSC) gate on the BD FACSCantoTM II (BD Biosciences). Data were analysed by BD CellQuestTM Pro software, version 5.2 (BD Biosciences). Lymphocytes were identified from a FSC/SSC scattergram. Binding of $CD20^+$ B cells by Hu8G10 or anti-CD22 antibody was identified using anti-CD20 PE versus Hu8G10 FITC or anti-CD20 PE versus anti-CD22 Alexa 647 cytogram plots respectively. A similar procedure was utilized to assess binding of anti-CD79b antibody to cynomolgus monkey peripheral blood B cells. Anti-CD79b antibody and human IgG isotype control (Genentech, Inc.) were labelled with Zenon Alexa Fluor 647 Human IgG Labelling Kit (Invitrogen) according to the manufacturer's protocol.

Analysis of peripheral blood B, Tand NK cells

Peripheral blood samples from cynomolgus monkeys were stained with saturating concentrations of fluorescently conjugated mAbs to human CD3, CD8, CD20 and CD45 (all cross-react with cynomolgus monkey leukocytes), and with appropriate isotype controls. Samples were incubated on ice, washed twice with FACS staining buffer and re-suspended in fixative buffer before acquisition. Flow cytometric acquisition was performed on the BD FACSCantoTM II on the day of staining. Data were analysed with BD FACSDivaTM software, version 6.1.1 (BD Biosciences). Flow cytograms were generated to establish the fraction of cells expressing each cell surface marker (expressed as percentage of FSC/SSC-gated lymphocytes). B cells were defined as $CD3^-CD20^+$ cells, T-cells as $CD3^+$ cells (cytotoxic T-cells as $CD3^+CD8^+$ cells, helper T-cells as $CD3^+CD8^-$ cells), and NK cells as $CD3^-CD20^-$ cells. For each sample at each time point for each lymphocyte subset, the absolute cell count was calculated based on % gated data generated by flow cytometry multiplied by the total lymphocyte count. Statistical analysis was not performed due to the low number of animals assigned to each dose group. All antibodies (anti-CD3, anti-CD8, anti-CD20 and anti-CD45) were purchased from BD Biosciences.

Analysis of Ki-67 expression

The Ki-67 antibody binds to the protein pKi-67, which is expressed exclusively in proliferating cells (Schlüter *et al.*, 1993). Peripheral blood samples were stained with saturating concentrations of a fluorescently conjugated mAb to CD20. Cells were then washed, fixed and permeabilized using Dako IntraStain (Dako, Carpinteria, CA, USA) and stained with an antibody against the intracellular Ki-67 (BD Biosciences). Flow cytometric acquisition was performed on a FACSCaliburTM (BD Biosciences) on the day of staining. Data were analysed with FlowJoTM software, version 8.8.7 (Tree Star, Inc., Ashland, OR, USA). Lymphocytes were gated by FSC/SSC, and subsets of $CD20^+$ and $CD20^-$ lymphocytes were evaluated for expression of Ki-67, with positivity based on comparison to isotype control. Absolute counts of $Ki\text{-}67^+$ and $Ki\text{-}67^-$ B cells were determined by multiplying the percentage of each subset by the absolute B-cell count for each animal at each time point. Statistical analysis was not performed due to low number of animals assigned to each dose group.

Histopathology studies

In a separate anti-CD22 ADC study, cynomolgus monkeys of Mauritian origin were obtained from Covance, Inc and randomized by weight into groups. Five males and five females per group were administered a single i.v. injection of vehicle (control) or 6 $mg{\cdot}kg^{-1}$ anti-CD22 ADC on Day 1. Necropsies were performed on Day 8; all tissues (including the spleen) were collected for routine histopathological evaluation.

In a separate anti-CD79b ADC study, cynomolgus monkeys of Chinese origin were obtained from Charles River Laboratories International, Inc and randomized by weight into groups. Five males and five females per group were administered i.v. injections of vehicle (control) or 5 $mg{\cdot}kg^{-1}$ anti-CD79b ADC once every 3 weeks for a total of four doses. Necropsies were performed 1 week after the last dose on Day 71; all tissues (including the spleen) were collected for routine histopathological evaluation.

Spleen sections were fixed in 10% neutral-buffered formalin, routinely processed and embedded in paraffin. Sections were cut at 4–5 μM and stained with haematoxylin and eosin (H&E) for routine histopathological evaluation. Germinal centres (GCs) within splenic lymphoid follicles were specifically evaluated. GCs are identified on H&E-stained sections by their paler basophilic staining characteristics compared with the rest of the lymphoid follicle.

Bioanalysis of serum anti-CD22 and anti-CD79b ADCs

Anti-CD22 ELISA. Concentrations of unconjugated antibody following a single i.v. administration of unconjugated anti-CD22 antibody and total antibody (fully conjugated, partially deconjugated and fully deconjugated antibodies) following a single i.v. administration of anti-CD22 ADC were determined in serum by ELISA as described previously (Kaur *et al.*, 2013; Li *et al.*, 2013). The assay measures only antibodies with at least one intact complementarity determining region and fragment antigen-binding region. Briefly, anti-CD22 standards and samples diluted in sample diluent were incubated for 2 h with biotinylated sheep anti-human IgG antibody (Genentech, Inc.) and goat anti-human IgG antibody conjugated to horseradish peroxidase either in micronic tubes (National Scientific, Claremont, CA, USA) or polypropylene round-bottom plates (Corning Costar, Corning, NY, USA) to form a

bridging complex. Subsequently, these complexes were transferred to NeutrAvidin-coated plates (Thermo Fisher Scientific Inc., Waltham, MA, USA) and incubated for 1 h. After washing, the detection step was conducted using tetramethylbenzidine (TMB) substrate (Kirkegaard & Perry Laboratories, Inc., Gaithersburg, MD, USA). Absorbance was measured at 450 nm against a reference wavelength of 620 nm. The minimum quantifiable concentration was 63 ng·mL^{-1}.

Anti-CD79b ELISA. Concentrations of unconjugated antibody following a single i.v. administration of unconjugated an-CD79b antibody and total antibody (fully conjugated, partially deconjugated and fully deconjugated antibodies) following a single i.v. administration of anti-CD79b ADC were determined in serum by ELISA (Kaur *et al.*, 2013). The assay detects antibodies having at least one intact complementarity determining region and fragment antigen-binding region. Microtitre plates (96-well) (Nunc, Thermo Fisher Scientific Inc., Waltham, MA, USA) were coated with a 21-mer peptide of the extracellular domain of cynomolgus monkey CD79b (Genentech, Inc.) in coat buffer (PBS). After an overnight incubation at 4°C, plates were washed and treated with block buffer (PBS, 0.5%BSA, 0.05% polysorbate 20, 0.05% ProClin 300) for 1–2 h. Serum samples were then added to the plates and incubated at room temperature (RT) for 2 h. Plates were then washed and incubated for 1 h with biotinylated sheep anti-human IgG antibody (Genentech, Inc.) followed by streptavidin conjugated to horseradish peroxidase (GE Healthcare Life Sciences, Marlborough, MA, USA). After washing, the detection step was conducted using TMB substrate. Absorbance was measured at 450 nm against a reference wavelength of 620 nm. The minimum quantifiable concentration was 60 ng·mL^{-1}.

Antibody-dependent cellular cytotoxicity (ADCC)

The ability of anti-CD22 and anti-huCD79b antibodies to induce antibody-dependent cellular cytotoxicity (ADCC) was assessed *in vitro*. Peripheral blood mononuclear cells (PBMCs) from healthy human donors were used as effector cells, and a human Burkitt's lymphoma cell line (BJAB; Genentech Inc.) was used as target cells. Cells were counted and viability was determined by Vi-Cell™ (Beckman Coulter, Brea, CA, USA).

Briefly, PBMCs were isolated by density gradient centrifugation using Uni-Sep blood separation tubes (Accurate Chemical & Scientific, Westbury, NY, USA). Target cells in assay medium (RPMI 1640 medium with 10% FBS) were seeded in a 96-well, round-bottom plate. Serial dilutions of test and control antibodies were added to the plates containing the target cells, followed by incubation at 37°C with 5% CO_2 for 30 min to allow opsonization. After the incubation, PBMC effector cells in assay medium were added to each well at an effector-to-target cell ratio of 25:1, and the plates were incubated for 4 h. The plates were then centrifuged, and the activity of LDH in supernatants determined using Cytotoxicity Detection Kit (Roche Diagnostics, Indianapolis, IN, USA). The LDH reaction mixture was added to the supernatants, and the plates were incubated at RT for 15 min with shaking. The reaction was terminated with 1 M H_3PO_4 and absorbance was measured at 490 nm against a reference wave length of 650 nm. Absorbance of wells containing only the target cells served as the control for background (low control), whereas wells containing target cells lysed with Triton-X100 provided maximum achievable signal (high control).

ADCC activity is presented as the ratio of sample signal to the maximum achievable signal (%ADCC). Antibody-independent cellular cytotoxicity (AICC) was measured in wells containing target and effector cells without the addition of antibody. The extent of specific ADCC was calculated as follows:

$$\%\mathrm{ADCC} = 100 \cdot \frac{\mathrm{A}^{490\mathrm{nm}}(\mathrm{Sample})\ \mathrm{A}^{490\mathrm{nm}}(\mathrm{AICC})}{\mathrm{A}^{490\mathrm{nm}}(\mathrm{High\ Control})\ \mathrm{A}^{490\mathrm{nm}}(\mathrm{Low\ Control})}$$

ADCC values of sample dilutions were plotted against the antibody concentration and the dose–response curves fitted with a four-parameter model.

Complement-dependent cellular cytotoxicity (CDC)

The ability of anti-CD22 and anti-huCD79b antibodies to induce complement-dependent cytotoxicity (CDC) was assessed *in vitro*. The human lymphoma BJAB cell line was used as target cells. Complement was derived from either normal human (Quidel Corporation, Santa Clara, CA, USA) or rabbit serum (Calbiochem, Billerica, MA, USA). CDC activity was determined in a cell-viability assay, in which a reduction of the signal indicates the extent of cytotoxicity of anti-CD22, anti-huCD79b and rituximab (the positive control) antibodies.

Cells were counted, and viability was determined by Vi-Cell. The test and control antibodies were serially diluted in assay medium and aliquoted into a white 96-well, flat-bottom tissue culture plate (Corning Costar, Corning, NY, USA). After the addition of serum complement and the target cells, the plate was incubated at 37°C with 5% CO_2 for 2 h followed by 10–15 min incubation at RT. CellTiter-Glo reagent (Promega, Madison, WI, USA) was then added, and the plate was incubated at RT for 10 min with shaking. The extent of cell lysis was quantified by measuring the intensity of luminescence. Luminescence values of sample dilutions were plotted against the antibody concentration, and the dose–response curves were fitted with a four-parameter model.

Statistical analysis

Statistical analysis were not performed due to limited sample size per study group (n = 4 animals per group) in both anti-CD22 and anti-CD79b ADC studies.

Pharmacokinetic analysis

Serum concentration-time profiles were used to estimate the observed maximum serum concentration (Cmax), total drug exposure defined as AUC extrapolated to infinity (AUCinf), volume of distribution at steady state (Vss) and clearance (dose/AUC_{inf}). A non-compartmental analysis (Model 201, WinNonlin®Pro, Version 5.2.1; Pharsight Corporation; Mountain View, CA, USA) was used to describe the observed serum concentration data for anti-CD79b antibody; a two-compartment model with i.v.-bolus input, first-order elimination and macro-rate constants (Model 8, WinNonlin Pro, Version 5.2.1; Pharsight Corporation) was used to describe the observed serum concentration data for anti-CD22 antibody. Model selection was based on goodness of fit by visual

inspection and by the between-model comparison of Akaike's information criterion. PK parameters were analysed for each animal separately, and results for each dose group are summarized as mean ± SD.

Results

Binding of anti-CD22 and anti-CD79b antibodies to cynomolgus monkey B cells

Binding of the anti-CD22 and anti-CD79b antibodies to cynomolgus monkey B cells was determined with flow cytometry. Anti-CD22 bound to peripheral blood B cells in all animals of Indonesian ($n = 120$) and Mauritian origin ($n = 10$) (Figure 1). In contrast, anti-CD22 bound to peripheral blood B cells in 30% of animals of Chinese (3 of 10 tested) and Cambodian (3 of 10 tested) origin; in the rest of these animals, the binding was variable from low to absent (Figure 1). Hu8G10, a humanized antibody that binds to CD22 at an epitope distinct from the clinical candidate anti-CD22 antibody, bound to B cells of all tested animals. Given the consistent binding of anti-CD22 antibody to B cells in animals of Mauritian origin, these animals were used in studies evaluating PK and toxicology of anti-CD22 ADC. Before initiation of studies, binding of anti-CD22 antibody to B cells in all enrolled animals was confirmed. Similar selective binding of anti-CD79b antibody to B cells of animals of different origins was not observed, thus allowing the use of Chinese origin monkeys for studies involving CD79b.

Depletion of circulating CD20⁺ B cells following administration of anti-CD22 or anti-CD79b ADCs in ADC studies

To examine the *in vivo* pharmacodynamic effects of the anti-CD22 and anti-CD79b ADCs in Mauritian and Chinese cynomolgus monkeys respectively, levels of peripheral blood lymphocyte subsets were assessed over time. Animals were administered anti-CD22 ADC, anti-CD79b ADC, the respective unconjugated antibodies or vehicle.

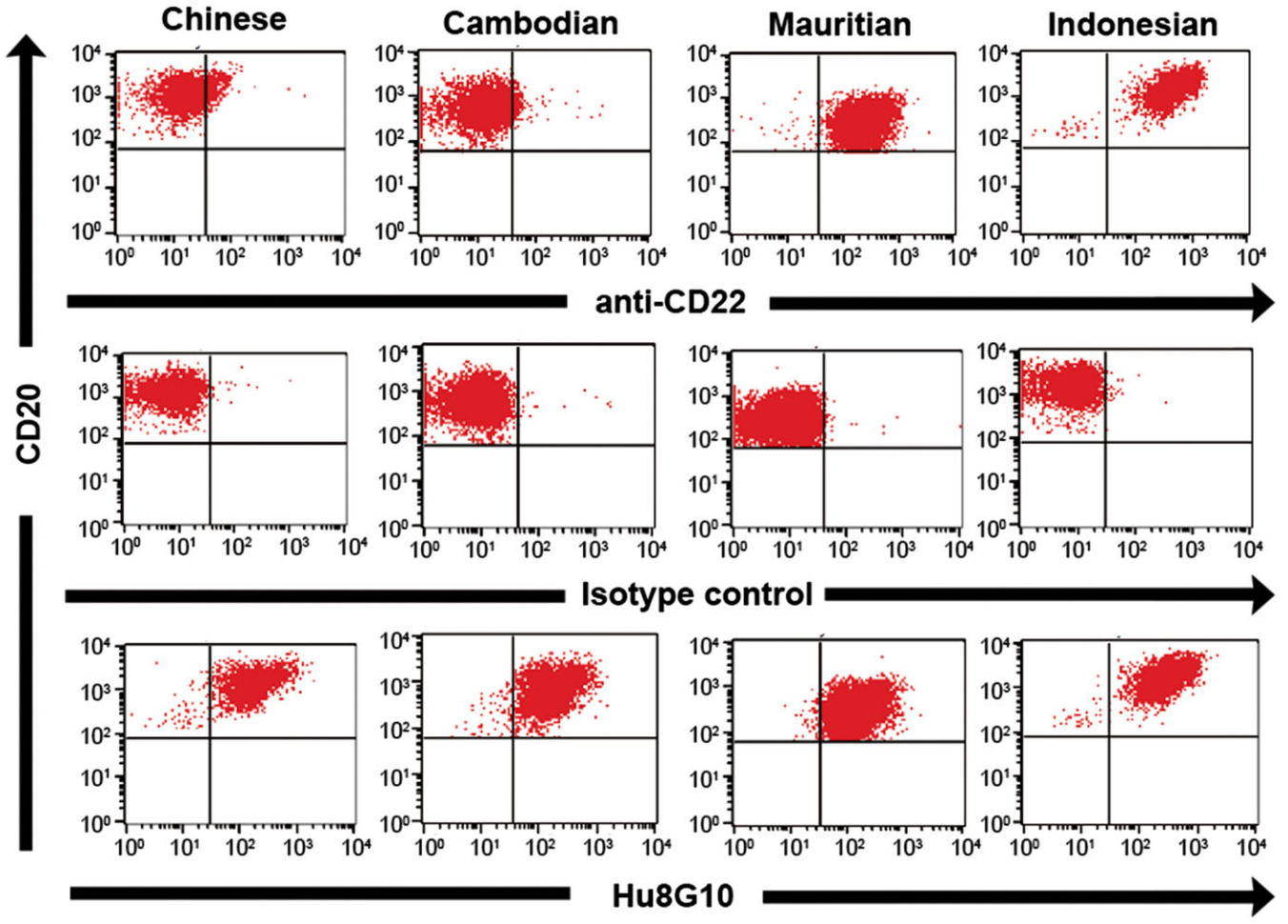

Figure 1

Anti-CD22 antibody binding to CD20⁺ B cells of cynomolgus monkeys of Chinese, Cambodian, Mauritian and Indonesian origins. Representative flow cytometry scatter plots of anti-CD22 antibody (upper panel), isotype control (middle panel) or Hu8G10 (lower panel) on gated CD20⁺ B cells in the peripheral blood from cynomolgus monkeys of different origins are presented.

Depletion of circulating B cells was observed in animals administered either ADC or the respective unconjugated antibody (Figure 2). Earlier recovery to baseline of levels of circulating B cells was observed in animals administered the unconjugated antibodies (Day 22 for anti-CD22 antibody and Day 30 for anti-CD79b antibody) compared with animals administered the ADCs (Day 45 for both anti-CD22 and anti-CD79b ADCs) (Figure 2). There was limited to no apparent depletion of peripheral blood $CD20^+$ B cells in animals administered vehicle. Depletion of peripheral blood $CD3^+$, $CD3^+CD4^+$ or $CD3^+CD4^-$ T-cells was not observed in any animal administered any test article or control vehicle.

Depletion of $CD20^+Ki\text{-}67^+$ B cells following administration of anti-CD22 or anti-CD79b ADCs in ADC studies

To evaluate the ability of the anti-CD22 and anti-CD79b ADCs to deplete proliferating cynomolgus monkey B cells, levels of peripheral blood $Ki\text{-}67^+$ B cells were determined. Animals were administered anti-CD22 ADC, anti-CD79b ADC, the respective unconjugated antibodies or vehicle.

In cynomolgus monkeys, although the percentage of $CD20^+Ki\text{-}67^+$ B cells in animals of Indonesian origin was slightly higher than that of animals of Chinese or Mauritian origins, the overall range in values across cynomolgus monkey origins were similar (Figure 3A and B). In Mauritian animals administered anti-CD22 ADC, a preferential depletion of $CD20^+Ki\text{-}67^+$ B cells was observed on Day 15 (median 0.3% of baseline for $CD20^+Ki\text{-}67^+$ vs. 45.0% of baseline for $CD20^+Ki\text{-}67^-$); this preferential depletion was not observed on Day 22 (Figure 3C). In contrast, preferential depletion was not observed in animals administered unconjugated antibody or vehicle on either day. Additionally, depletion of $CD20^-Ki\text{-}67^+$ non-B lymphocytes (including T, NK and NK T-cells) was not observed in animals administered vehicle, unconjugated anti-CD22 antibody or anti-CD22 ADC (data not shown). This finding demonstrated the specificity of the anti-CD22 ADC for proliferating B cells.

Similar assessments of circulating $CD20^+Ki\text{-}67^+$ B cells were performed on Chinese animals administered vehicle, unconjugated anti-CD79b antibody or anti-CD79b ADC (Figure 3D). Similar to animals administered anti-CD22 ADC, a preferential depletion of $CD20^+Ki\text{-}67^+$ B cells was observed on Day 15 following administration of anti-CD79b ADC (median 1.1% of baseline for $CD20^+Ki\text{-}67^+$ vs. 23.6% of baseline for $CD20^+Ki\text{-}67^-$). Preferential depletion was not observed on Day 22. In contrast, preferential depletion was not observed in animals administered the unconjugated anti-CD79b antibody or vehicle on either day. Additionally, preferential depletion of $CD20^-Ki\text{-}67^+$ non-B lymphocytes was not observed in animals administered vehicle, anti-CD79b antibody or anti-CD79b ADC (data not shown).

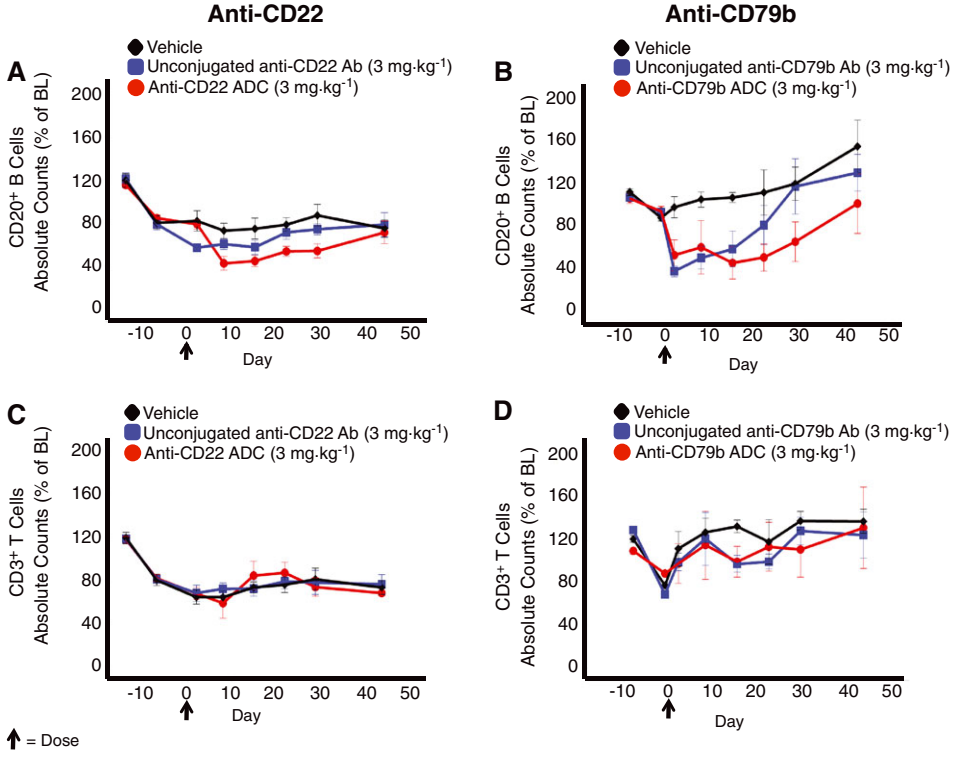

Figure 2

Depletion of $CD20^+$ B cells following administration of anti-CD22 or anti-CD79b ADCs. Peripheral blood $CD20^+$ B cells (panels A and B) or $CD3^+$ T-cells (panels C and D) in animals administered either anti-CD22 (panels A and C) or anti-CD79b (panels B and D) ADCs ($n = 4$); respective unconjugated antibodies (Ab) ($n = 4$) or vehicle ($n = 4$) over time are presented. Data presented are group mean absolute counts expressed as a percentage of baseline (% of BL) at each time point. Baseline was calculated as the average value obtained at two pre-dose time points (shown). Error bars represent SEM. The arrow denotes administration of the test substances.

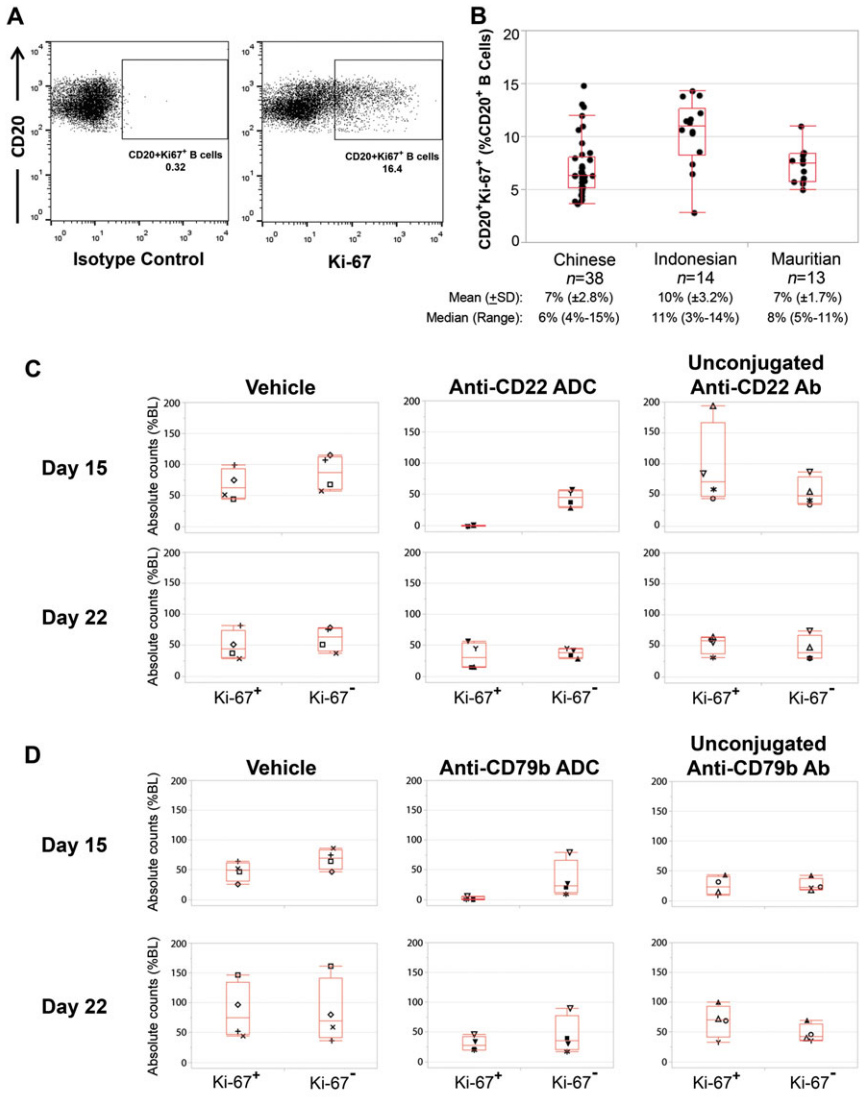

Figure 3

Baseline percentage of peripheral blood Ki-67$^+$ B cells in cynomolgus monkeys of Indonesian, Chinese and Mauritian origins. Percentage of peripheral blood CD20$^+$Ki-67$^+$ B cells expressed as a percentage of total CD20$^+$ B cells in cynomolgus monkeys is presented. (A) Representative cytogram of CD20$^+$Ki-67$^+$ B cells gated per respective isotype control. (B) Box plot with the individual animal distribution within each animal origin. The upper, middle and lower lines of each box represent the 75th quartile, median and 25th quartile respectively. Mean percentage (±SD), median and range of peripheral blood CD20$^+$Ki-67$^+$ B cells tabulated by animal origin are shown. (C) Single i.v. doses of vehicle (left panel), 3 mg·kg^{-1} anti-CD22 ADC (middle panel), or 3 mg·kg^{-1} unconjugated anti-CD22 antibody (Ab) (right panel) were administered to cynomolgus monkeys. Absolute numbers of Ki-67$^+$ and Ki-67$^-$ B cells are plotted as a percentage of the average pre-dose value for each animal (symbols) on Day 15 (upper panel) and Day 22 (lower panel). Boxes show the individual animal distribution within each group, where the upper, middle and lower lines represent the 75th quartile, median and 25th quartile respectively. (D) Single i.v. doses of vehicle (left panel), 3 mg·kg^{-1} anti-CD79b ADC (middle panel), or 3 mg·kg^{-1} unconjugated anti-CD79b antibody (Ab) (right panel) were administered to cynomolgus monkeys. Absolute numbers of Ki-67$^+$ and Ki-67$^-$ B cells are plotted as a percentage of the average pre-dose value for each animal (symbols) on Day 15 (upper panel) and Day 22 (lower panel). Boxes show the individual animal distribution within each group, where the upper, middle and lower lines represent the 75th quartile, median and 25th quartile respectively.

Histological evaluation of spleen confirms depletion of GC lymphocytes in histopathology studies

To determine the effects of anti-CD22 and anti-CD79b ADCs on proliferating lymphocytes in tissues, histological evaluation of spleen from animals administered anti-CD22 ADC, anti-CD79b ADC or vehicle was performed. In agreement with the observed depletion of proliferating CD20$^+$Ki-67$^+$ B cells in circulation, a loss of GCs within splenic lymphoid follicles was observed in all animals administered anti-CD22 ADC (Figure 4A) or anti-CD79b ADC (Figure 4B). Similar loss of GCs within the splenic lymphoid follicles was not observed in animals administered with vehicle control. Similar loss of GCs within the splenic lymphoid follicles was not observed in animals administered with vehicle control.

Pharmacokinetics of anti-CD22 and anti-CD79b ADCs in ADC studies

To determine the extent of exposure of ADCs and unconjugated antibodies, serum antibody concentrations were measured in animals following i.v. administration of anti-CD22 or anti-CD79b ADCs and their respective unconjugated antibodies. Mean serum concentrations over time are presented in Figure 5.

Serum concentrations of the unconjugated antibody after a single i.v. administration of unconjugated anti-CD22 antibody or total antibody (fully conjugated, partially deconjugated and fully deconjugated antibodies) after a single i.v. administration of anti-CD22 ADC were at maximum levels immediately after dosing (Figure 5). Subsequently, the concentrations declined over time in a bi-exponential manner as expected for a therapeutic monoclonal antibody. None of the animals administered vehicle had measurable serum concentrations of anti-CD22 antibody (data not shown). Systemic exposure (AUCinf) of unconjugated anti-CD22 antibody was about two times higher than that of the total antibody after ADC administration, and the Vss of unconjugated antibody was approximately two times smaller than that of the total antibody after ADC administration (Table 1). These data suggest a modest effect of the MMAE conjugation on the antibody clearance; at the same dose level, the total antibody following i.v. ADC administration cleared about two times faster than unconjugated antibody. The clearance (CL) of unconjugated anti-CD22 antibody (Table 1) in the current study is typical and comparable with other IgG1 monoclonal antibodies in monkeys (Bumbaca Yadav *et al.*, 2015). Both unconjugated and total antibodies remained detectable for the entire duration of the study (until Day 44) (Figure 5A).

Similar to anti-CD22 antibody, the PK profiles of unconjugated antibody following a single i.v. administration of unconjugated anti-CD79b antibody and total antibody following a single i.v. administration of anti-CD79b ADC were bi-exponential as expected for a therapeutic monoclonal antibody. (Figure 5B). Exposure of unconjugated anti-CD79b antibody was also slightly higher than that of total antibody after ADC administration. The Vss of unconjugated anti-CD79b antibody was comparable with that of total antibody; the Vss of both unconjugated and total antibodies approximated the plasma volume of a monkey (Davies and Morris, 1993), suggesting majority of unconjugated antibody and total antibody were retained in the central or plasma compartment after a single dose of 3 mg·kg^{-1} unconjugated anti-CD79b or anti-CD79b ADC. The AUCinf for unconjugated anti-CD79b antibody was comparable with that of the total antibody (Table 1). Unlike anti-CD22 antibody (Figure 5A), unconjugated anti-CD79b antibody and total anti-CD79b antibody levels were both below the level of detection after Day 14 (Figure 5B). This suggests that a greater contribution of a specific (B-cell mediated) CL component

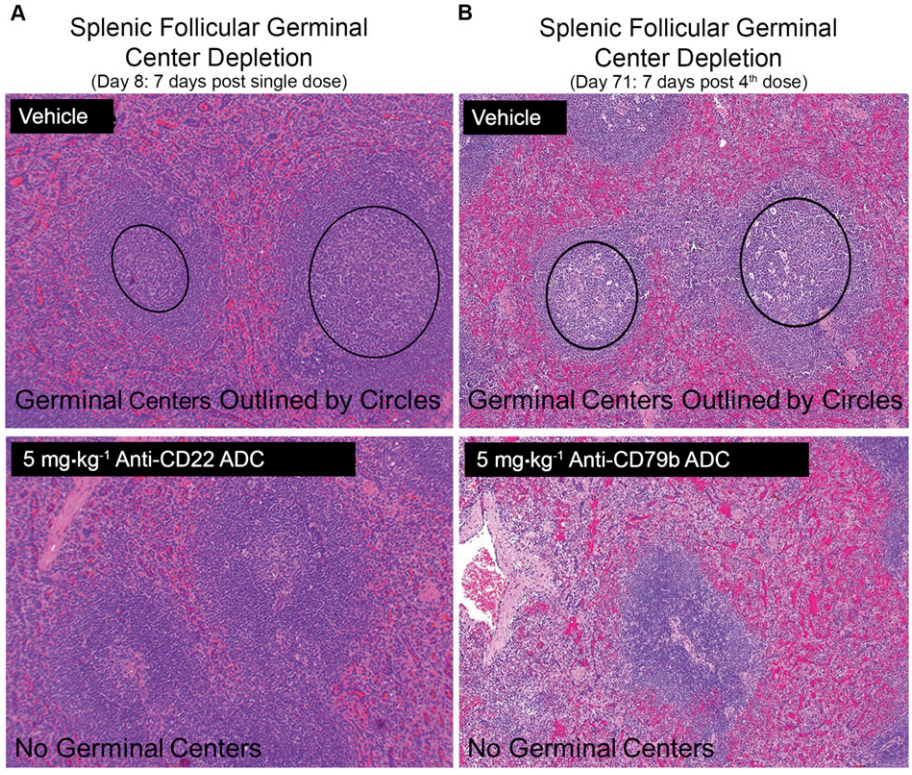

Figure 4

Depletion of germinal centers in lymphoid tissues of cynomolgus monkeys administered anti-CD22 ADC or anti-CD79b ADC. (A) Representative H&E-stained section of spleen from animals administered single i.v. doses of either vehicle (upper panel) or 6 mg·kg^{-1} anti-CD22 ADC (lower panel) on Day 8 is presented. (B) Representative H&E-stained section of spleen from animals administered four i.v. doses of vehicle (upper panel) or 5 mg·kg^{-1} anti-CD79b ADC (lower panel) on Day 71 (7 days following fourth dose) is presented.

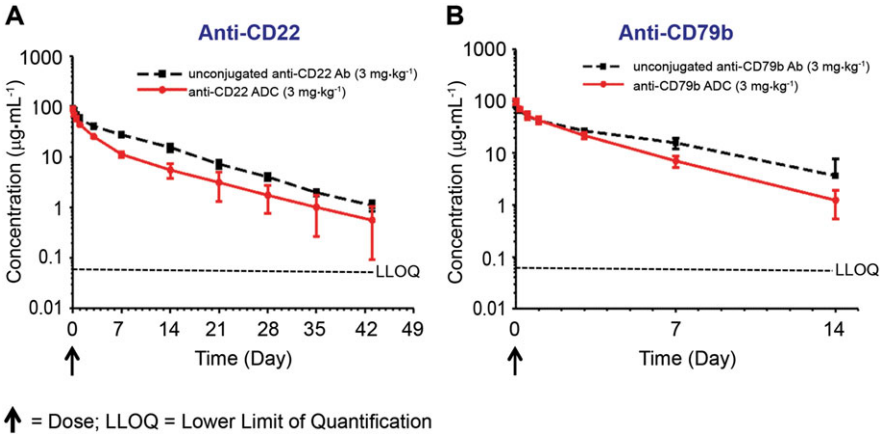

Figure 5

Systemic exposure of anti-CD22 antibody is slightly higher than that of anti-CD79b antibody. Group mean (±SD) serum concentrations of antibody following a single i.v. administration of 3 mg·kg^{-1} unconjugated anti-CD22 antibody (Ab) or anti-CD22 ADC (A) or 3 mg·kg^{-1} unconjugated anti-CD79b antibody or anti-CD79b ADC (B) are presented. Red solid line represents serum concentration of total (both conjugated and unconjugated) antibody in animals administered ADC. Black dashed line represents serum concentration of unconjugated antibody in animals administered the respective unconjugated antibody.

Table 1

Group mean (±SD) values of pharmacokinetic parameters for unconjugated or total antibodies (Ab) after a single i.v. administration of unconjugated anti-CD22 antibody, unconjugated anti-CD79b antibody or the respective ADCs at 3 mg·kg^{-1} to cynomolgus monkeys

	Anti-CD22		Anti-CD79b	
PK parameters	**Unconjugated Ab**	**Total Ab**	**Unconjugated Ab**	**Total Ab**
C_{max}(µg·mL^{-1})	95.8 ± 3.00	80.6 ± 7.39	82.5 ± 4.93	98.3 ± 13.4
AUC_{inf}(µg·day^{-1}·mL^{-1})	606 ± 43.9	325 ± 48.7	289 ± 54.6	217 ± 36.1
V_{ss}(mL·kg^{-1})	51.8 ± 1.59	80.0 ± 14.9	45.7 ± 3.36	43.1 ± 3.02
CL(mL·day^{-1}·kg^{-1})	4.97 ± 0.352	9.39 ± 1.46	10.6 ± 1.86	14.2 ± 2.60

to total CL of the anti-CD79b antibody than that of anti-CD22 antibody, and a significant concentration drop in the terminal phase is most likely due to target mediated elimination (Mager, 2006). Thus, systemic exposure of anti-CD22 antibody is greater compared with anti-CD79b antibody. The Cmax of total antibody post i.v. administration of anti-CD22 and anti-CD79b ADCs and their respective unconjugated antibodies were similar, which confirmed that all animals received the same dose, and the initial drug distribution was comparable (Table 1).

ADCC and CDC activity of anti-CD22 and anti-huCD79b antibodies

To determine the role of effector functions in the MOA of the anti-CD22 and anti-huCD79b antibodies, the ADCC and CDC were measured *in vitro*. ADCC is an effector function in which antigen-specific antibodies direct effector cells of the innate immune system to kill antigen-expressing target cells. CDC is a cell-killing mechanism in which complement-dependent cell lysis occurs due to binding of the antibody to the antigen on a cell surface and subsequent activation of the complement pathway.

Dose–response curves from representative ADCC experiments are presented in Figure 6. While rituximab (positive control) demonstrated robust ADCC in BJAB cells, there was no apparent ADCC with anti-CD22 antibody, and only moderate ADCC with anti-huCD79b antibody. Anti-CD22 and anti-huCD79b antibodies did not have detectable CDC in BJAB cells with either human or rabbit complement (data not shown).

Discussion

The development of humanized and fully human mAbs as therapeutics for the treatment of cancer has vastly improved clinical outcomes. These new therapeutics provide a more targeted and specific approach than nonspecific elimination of proliferating cells via chemotherapeutic agents. The depletion of circulating malignant cells by targeted antibodies can include multiple physiological processes in blood, including antibody-mediated opsonization, ADCC and/or CDC. However, antibodies that are effective in circulation may not always demonstrate similar potency in tissues, where these mechanisms may be less effective than they are

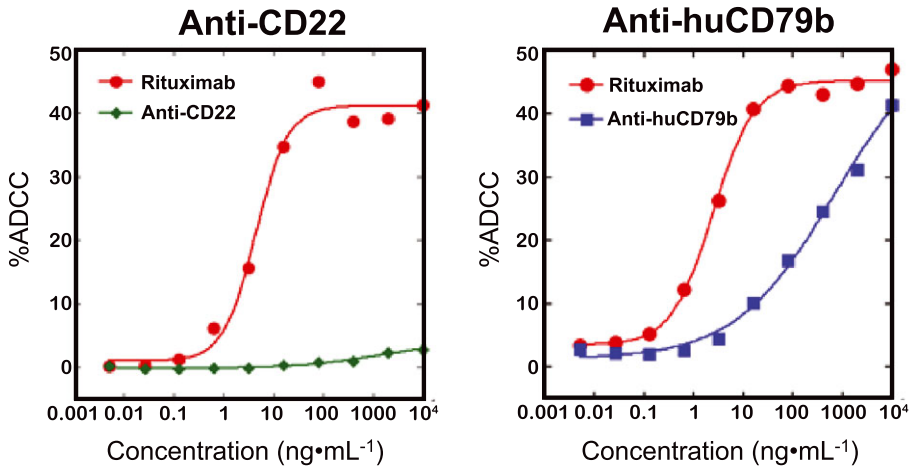

Figure 6

ADCC activity of anti-CD22 and anti-huCD79b antibodies. Anti-CD22 antibody, anti-huCD79b antibody and rituximab (positive control) were evaluated for their ability to induce ADCC in human BJAB. Each figure represents the results from three independent experiments conducted with each antibody using peripheral blood mononuclear cells from different donors. The % ADCC was plotted against concentration of the antibodies and data fitted with a four-parameter model.

in blood (Townsend *et al.,* 2010). For example, rituximab can deplete circulating B cells to near-undetectable levels within days following administration. In contrast, B cells in tissues are depleted less efficiently and can require a longer time for maximum depletion (Maloney *et al.,* 1997; Thurlings *et al.,* 2008).

Conjugation of cytotoxic agents to mAbs can further increase the effectiveness of both mAbs and cytotoxic agents. The mAb component of an ADC delivers a cytotoxic agent to malignant tissue by specifically targeting malignant cells. As a consequence, the concentration of the cytotoxic agent in malignant cells is increased and leads to increased potency. This overcomes both the lack of specificity of cytotoxic agents and the limited potency of the therapeutic antibodies alone. In addition, this targeted approach potentially reduces nonspecific systemic effects of cytotoxic agents by decreasing their access to normal tissues. We took advantage of this concept by conjugating potent cytotoxic agent to antibodies targeting CD22 and CD79b on B cells. Upon binding to CD22 or CD79b, these ADCs are rapidly internalized and subsequently release MMAE in the targeted cell.

We demonstrated specific targeting and elimination of B cells in cynomolgus monkey blood and tissue by both anti-CD22 and anti-CD79b ADCs at dose levels that were well tolerated. Initial depletion of B cells in blood was comparable between the ADCs and the respective unconjugated antibodies and was likely mediated by antibody opsonization.

The increased depletion of B cells by unconjugated anti-CD79b antibody (~75% reduction compared with baseline) compared with unconjugated anti-CD22 antibody (~50% reduction compared with baseline) is likely related to multiple factors not yet fully understood. Although the overall systemic exposure of unconjugated anti-CD79b is about two times lower than that of unconjugated anti-CD22, the initial peak concentrations (C_{max}) of the two unconjugated antibodies were similar; therefore, it is less likely the difference of the initial B depletion is due to the exposure difference of the two unconjugated antibodies. The greater *in vitro* ADCC observed with the former and/or signalling through CD79b may be contributing factors (Figure 6).

The anti-CD22 and anti-CD79b ADCs are not expected to affect proliferating haematopoetic stem cells, as these cells do not express CD22 or CD79b. This is supported by the rapid recovery of B cells in circulation after clearance of the ADCs, thus suggesting that the pool of stem cells remained unperturbed. Furthermore, in agreement with antibody specificity, levels of proliferating and non-proliferating T and NK cells were not affected.

The anti-CD22 and anti-CD79b ADCs mediated an extended duration of B-cell depletion in blood compared with unconjugated antibodies. This effect was achieved despite the overall lower systemic serum exposure of ADCs, characterized by serum total antibody concentrations, than their respective unconjugated antibodies, suggesting that the difference in pharmacodynamic effects between the ADC and the unconjugated antibodies were mediated by a differential MOA, rather than just the exposure. The extended depletion of B cells was characterized by preferential depletion of proliferating Ki-67$^+$ B cells. The preferential depletion of proliferating Ki-67$^+$ compared with non-proliferating Ki-67$^-$ B cells was not observed on Day 22, by which time a majority of the ADCs had been cleared.

Before initiation of the pharmacokinetic/pharmacodynamic studies, binding of anti-CD22 and anti-CD79b antibodies to cynomolgus monkey B cells was confirmed by flow cytometry. Anti-CD22 antibody selectively bound to B cells from Indonesian or Mauritian animals. In contrast, binding to B cells from Chinese or Cambodian animals was limited. Preliminary sequence analysis of the CD22 gene in Chinese and Indonesian animals did not indicate differences of sufficient magnitude to account for these differences. Therefore, the observed binding selectivity of anti-CD22 antibody may be due to post-translational modification

of CD22 on the surface of B cells. This origin-specific binding of anti-CD22 antibody appeared to be specific to cynomolgus monkeys, as binding of anti-CD22 antibody to peripheral blood B cells from healthy human donors did not reveal any such specificity. Anti-CD22 antibody bound to $CD20^+$ B cells from all 157 donors (data not shown). Similar origin-specific binding was not observed with anti-CD79b, which bound to B cells from animals of all origins at comparable levels.

The specific depletion of proliferating B cells supports the potential therapeutic value of these ADCs, as published data point to the importance of the conjugated cytotoxic agent for optimal efficacy. An unconjugated anti-CD22 antibody epratuzumab requires high dose levels for efficacy (Leonard *et al.,* 2004). Rituximab, a non-internalized anti-CD20 antibody, requires robust ADCC for efficacy. In contrast, the anti-CD22 and anti-CD79b ADCs take advantage of internalization and subsequent release of the cytotoxic agent to improve the efficacy. As studies in xenograft models indicate, drug-independent mechanisms are not sufficient to mediate efficacy in and of themselves (Li *et al.,* 2013).

The successful progression of therapeutics from Phase III clinical studies to marketing approval has decreased to only ~50% in recent years (Arrowsmith, 2011; Arrowsmith and Miller, 2013). This attrition rate has largely been attributed to lack of efficacy and highlights the need for understanding MOA and pharmacological activity at early stages of development (Cook *et al.,* 2014). Anti-CD22 and anti-CD79b ADCs were effective in mouse xenograft models (Dornan *et al.,* 2009; Polson *et al.,* 2010). They specifically target proliferating B cells in both blood and tissue in cynomolgus monkeys at a dose level that was well tolerated. These findings increase our confidence in potential efficacy of anti-CD22 and anti-CD79b ADCs in humans.

The pharmacology and MOA of anti-CD22 and anti-huCD79b ADCs make them promising therapeutics for the treatment of NHL. Both anti-CD22 and anti-huCD79b ADCs target Ki-67^+ B cells in lymphoid tissues and in circulation. Thus, these ADCs could effectively target proliferating malignant B cells in NHL and offer a more favourable risk–benefit profile than traditional chemotherapeutic agents. Indeed, the results of Phase I clinical studies with anti-CD22-MMAE (ClinicalTrial.gov identifier, NCT01209130) and anti-huCD79b-MMAE (ClinicalTrial.gov identifier, NCT01290549) in patients with relapsed/refractory NHL showed acceptable safety profiles, PK and anti-tumour activity (Palanca-Wessels *et al.,* 2015; Advani *et al.,* 2016).

Acknowledgements

The authors acknowledge the financial support of Genentech, a member of the Roche Group, for these studies. We would like to thank Dale Stevens and Amy Oldendrop for providing study monitor support to the anti-CD22 and anti-CD79b ADC studies. We would also like to thank Kathy Howell, Olivia Hwang and Clarissa David and Sock-Cheng Lewin-Koh for their assistance with flow cytometry analysis. Finally, we would like to thank Seattle Genetics for their technology in auristatin conjugation.

Author contributions

All of the listed authors contributed to the design, research, drafting and final approval of the work. They each agree to be accountable for all aspects of the work.

Conflict of interest

All authors are current or past employees of Genentech, Inc., a member of the Roche Group.

Declaration of transparency and scientific rigour

This Declaration acknowledges that this paper adheres to the principles for transparent reporting and scientific rigour of pre-clinical research recommended by funding agencies, publishers and other organisations engaged with supporting research.

References

Advani RH, Lebovic D, Chen A, Brunvand M, Goy A, Chang JE *et al.* (2016). Phase I study of the anti-CD22 antibody-drug conjugate pinatuzumab vedotin with/without rituximab in patients with relapsed/refractory B-cell non-Hodgkin's lymphoma. Clin Cancer Res. doi:10.1158/1078-0432.CCR-16-0772.

Alexander SPH, Kelly E, Marrion N, Peters JA, Benson HE, Faccenda E *et al.* (2015). The Concise Guide to PHARMACOLOGY 2015/16: Overview. Br J Pharmacol 172: 5729–5143.

Arrowsmith J (2011). Trial watch: phase III and submission failures: 2007–2010. Nat Rev Drug Discov 10: 87.

Arrowsmith J, Miller P (2013). Trial watch: phase II and phase III attrition rates 2011–2012. Nat Rev Drug Discov 12: 569.

Bumbaca Yadav D, Sharma VK, Boswell CA, Hotzel I, Tesar D, Shang Y *et al.* (2015). Evaluating the use of antibody variable region (Fv) charge as a risk assessment tool for predicting typical cynomolgus monkey pharmacokinetics. J Biol Chem 290: 29732–29741.

Burton JD, Goldenberg DM (2010). New agents and approaches to the treatment of B-cell non-Hodgkin lymphoma. Expert Opin Emerg Drugs 15: 569–583.

Cook D, Brown D, Alexander R, March R, Morgan P, Satterthwaite G *et al.* (2014). Lessons learned from the fate of AstraZeneca's drug pipeline: a five-dimensional framework. Nat Rev Drug Discov 13: 419–431.

Davies B, Morris T (1993). Physiological parameters in laboratory animals and humans. Pharm Res 10: 1093–1095.

Dornan D, Bennett F, Chen Y, Dennis M, Eaton D, Elkins K *et al.* (2009). Therapeutic potential of an anti-CD79b antibody-drug conjugate, anti-CD79b-vc-MMAE, for the treatment of non-Hodgkin lymphoma. Blood 114: 2721–2729.

Doronina SO, Toki BE, Torgov MY, Mendelsohn BA, Cerveny CG, Chace DF *et al.* (2003). Development of potent monoclonal antibody auristatin conjugates for cancer therapy. Nat Biotechnol 21: 778–784.

Institute of Laboratory Animal Research, National Research Council (1996). Guide for the Care and Use of Laboratory Animals. Available

at https://grants.nih.gov/grants/olaw/Guide-for-the-Care-and-Use-of-Laboratory-Animals.pdf (accessed 17 January 2017).

Kaur S, Xu K, Saad OM, Dere RC, Carrasco-Triguero M (2013). Bioanalytical assay strategies for the development of antibody–drug conjugate biotherapeutics. Bioanalysis 5: 201–226.

Kilkenny C, Browne W, Cuthill IC, Emerson M, Altman DG (2010). Animal research: Reporting *in vivo* experiments: the ARRIVE guidelines. Br J Pharmacol 160: 1577–1579.

Leonard JP, Coleman M, Ketas JC, Chadburn A, Furman R, Schuster MW*et al.* (2004). Epratuzumab, a humanized anti-CD22 antibody, in aggressive non-Hodgkin's lymphoma: phase I/II clinical trial results. Clin Cancer Res 10: 5327–5334.

Li D, Poon KA, Yu SF, Dere R, Go M, Lau J *et al.* (2013). DCDT2980S, an anti-CD22-monomethyl auristatin E antibody-drug conjugate, is a potential treatment for non-Hodgkin lymphoma. Mol Cancer Ther 12: 1255–1265.

Mager DE (2006). Target-mediated drug disposition and dynamics. Biochem Pharmacol 72: 1–10.

Maloney DG, Grillo-Lopez AJ, White CA, Bodkin D, Schilder RJ, Neidhart JA *et al.* (1997). IDEC-C2B8 (Rituximab) anti-CD20 monoclonal antibody therapy in patients with relapsed low-grade non-Hodgkin's lymphoma. Blood 90: 2188–2195.

McGrath JC, Lilley E (2015). Implementing guidelines on reporting research using animals (ARRIVE etc.): new requirements for publication in BJP. Br J Pharmacol 172: 3189–3193.

Palanca-Wessels MC, Czuczman M, Salles G, Assouline S, Sehn LH, Flinn I *et al.* (2015). Safety and activity of the anti-CD79B antibody-drug conjugate polatuzumab vedotin in relapsed or refractory B-cell non-Hodgkin lymphoma and chronic lymphocytic leukaemia: a phase 1 study. Lancet Oncol 16: 704–715.

Polson AG, Yu SF, Elkins K, Zheng B, Clark S, Ingle GS *et al.* (2007). Antibody-drug conjugates targeted to CD79 for the treatment of non-Hodgkin lymphoma. Blood 110: 616–623.

Polson AG, Calemine-Fenaux J, Chan P, Chang W, Christensen E, Clark S *et al.* (2009). Antibody-drug conjugates for the treatment of non-Hodgkin's lymphoma: target and linker-drug selection. Cancer Res 69: 2358–2364.

Polson AG, Williams M, Gray AM, Fuji RN, Poon KA, McBride J *et al.* (2010). Anti-CD22-MCC-DM1: an antibody-drug conjugate with a stable linker for the treatment of non-Hodgkin's lymphoma. Leukemia 24: 1566–1573.

Schlüter C, Duchrow M, Wohlenberg C, Becker MH, Key G, Flad HD *et al.* (1993). The cell proliferation-associated antigen of antibody Ki-67: a very large, ubiquitous nuclear protein with numerous repeated elements, representing a new kind of cell cycle- maintaining proteins. J Cell Biol 123: 513–522.

Shan D, Press OW (1995). Constitutive endocytosis and degradation of CD22 by human B cells. J Immunol 154: 4466–4475.

Sievers EL, Senter PD (2013). Antibody-drug conjugates in cancer therapy. Annu Rev Med 64: 15–29.

Southan C, Sharman JL, Benson HE, Faccenda E, Pawson AJ, Alexander SP *et al.* (2016). The IUPHAR/BPS Guide to PHARMACOLOGY in 2016: towards curated quantitative interactions between 1300 protein targets and 6000 ligands. Nucl Acids Res 44: D1054–D1068.

Sutherland MSK, Sanderson RJ, Gordon KA, Andreyka J, Cerveny CG, Yu C *et al.* (2006). Lysosomal trafficking and cysteine protease metabolism confer target-specific cytotoxicity by peptide-linked anti-CD30-auristatin conjugates. J Biol Chem 281: 10540–10547.

Thurlings RM, Vos K, Wijbrandts CA, Zwinderman AH, Gerlag DM, Tak PP (2008). Synovial tissue response to rituximab: mechanism of action and identification of biomarkers of response. Ann Rheum Dis 67: 917–925.

Townsend MJ, Monroe JG, Chan AC (2010). B-cell targeted therapies in human autoimmune diseases: an updated perspective. Immunol Rev 237: 264–283.

Zheng B, Fuji RN, Elkins K, Yu SF, Fuh FK, Chuh J *et al.* (2009). In vivo effects of targeting CD79b with antibodies and antibody-drug conjugates. Mol Cancer Ther 8: 2937–2946.